change in peak current as a function of melatonin concentration was evaluated using square wave voltammetry for both the modified and unmodified electrodes. Sqaure wave voltammograms recorded for different Mel concentrations ranging in between 100nM – 200μM in pH-7 phosphate buffer. A sharp peak at ~ 0.72V in SWV corresponds to the oxidation of melatonin at the bare surface[221]. Whereas, much facilitated Mel oxidation over AuNP-PLL/PND bio-interface was inferred from a shift of ~ 60mV in the peak potential. The shift in the peak potential or the electrocatalytic activity can be assigned to the selective interactions of Mel with the surface modification at the bio-interface leading to aided electron transfer and expedited oxidation at low potentials. Furthermore, with the bare electrode, the lowest concentration that could be visibly detected using SWV plots were found to be 1μM. Interestingly, the AuNP-PLL/PNDs/GCE showed a peak even at 10nM Mel concentration (Figure 4.8)

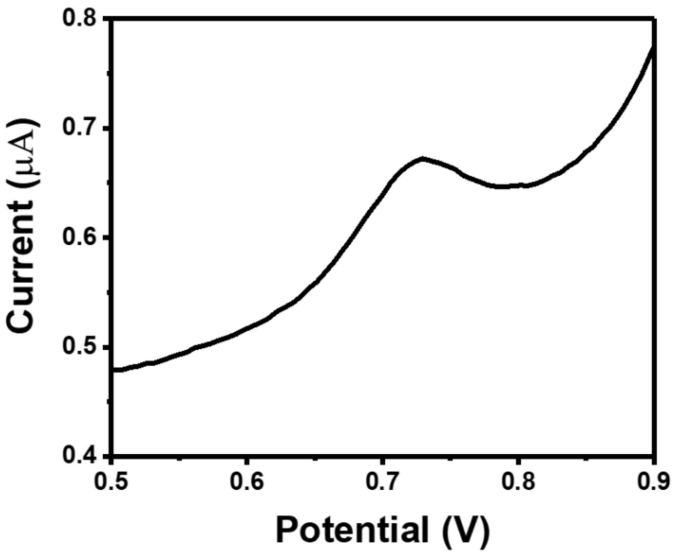

Figure 4.8 Square wave voltammogram of 10nM melatonin concentration

Nevertheless, the concentration dependency could be recognized only above 100nM Mel concentration. The inset of Figure 4.9 shows the linear increase in oxidation peak current Ip with an increase in the Mel concentration for both the bare and AuNP-PLL/PNDs/GCE electrode. However, it was found that the increase in the peak current with increasing concentration is much steeper at lower concentrations (till 25μM) compared to the higher ones. Therefore, the following two linear regression equations were used to express the dependence of Ip on Mel concentration for both the electrodes.

AuNP-PLL/PNDs/GCE: $Y= 0.043\ [0.1\text{-}25\mu M] + 0.2115, \quad R^2 = 0.9948$

$Y= 0.0213\ [50\text{-}200\mu M] + 0.789, \quad R^2 = 0.9998$

Bare GCE: $Y= 0.0194\ [1\text{-}25\mu M] + 0.0171, \quad R^2 = 0.9937$

$Y= 0.009\ [50\text{-}200\mu M] + 0.3818, \quad R^2 = 0.9948$

From the regression equations, it can be concluded that the fabricated bio-interface exhibited an increase of more than two fold in sensitivity compared to the bare electrode. Limit of detection (LOD) for bare and modified GCE was also calculated using 3S/σ, where S stands for a standard deviation of 'n' number of blank voltammograms and σ is the slope of the calibration plot. The LOD for modified GCE was found to be 31.6nM which is reasonably lower than the LOD of bare GCE, which is 120nM.

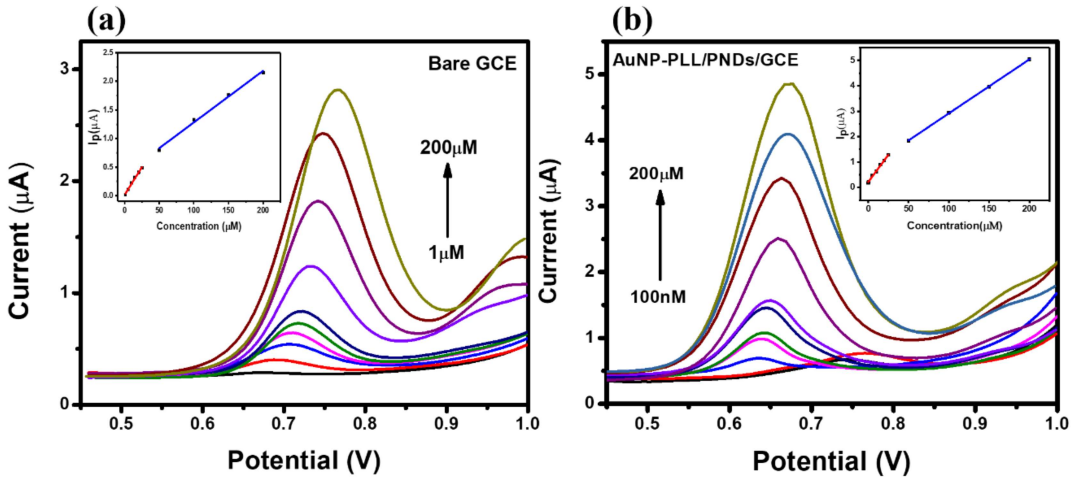

Figure 4.9 Concentration-dependent study: (a) Square wave voltammogram recorded for bare GCE for 1, 5μM, 10μM, 15μM, 20μM, 25μM, 50μM, 100μM, 150μM, 200μM Mel concentration, calibration plots shown in inset for Mel concentration from 1 μM to 200μM. (b) Square wave voltammograms recorded for AuNP-PLL/PNDs/GCE for 100nM, 500nM, 5μM, 10μM, 15μM, 20μM, 25μM, 50μM, 100μM, 150μM, 200μM Mel concentration, calibration plots shown in inset for Mel concentration from 100nM to 200μM

4.2.3.2 Effect of Square Wave Frequency

To study the nature of the mass-transfer process involved in the oxidation of Mel, variation in the oxidation peak current was recorded with increasing frequency (*f*) of the square wave. Figure 4.10 (a) shows the square wave voltammograms corresponding to 25μM Mel in pH-7 buffer with varying frequencies from 5-35Hz. The variation in peak current I_p was plotted as a function of *f* and $(f)^{1/2}$ (Figure 4.10,b) where I_p Vs. $(f)^{1/2}$ showed more linear regression relation in comparison to I_p Vs. *f*.

$$I_p\,(\mu A) = 0.0504\,f\,[5\text{-}35Hz] + 0.6754 \qquad R^2 = 0.9642$$

$$I_p\,(\mu A) = 0.4227\,f^{1/2}\,[5\text{-}35Hz] - 0.1356 \qquad R^2 = 0.9919$$

These results suggest that the oxidation of Mel is diffusion-controlled instead of involvement of any adsorption complications[222].

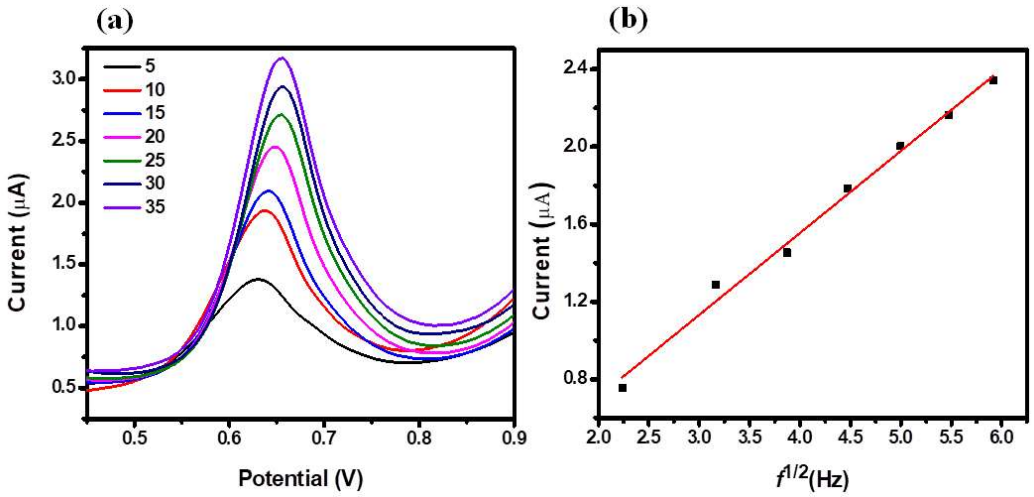

Figure 4.10 (a) Voltammograms for increasing square wave frequency on AuNPs-PLL/PNDs/GCE (b) shows the liner relation between Ip Vs (f) ½

4.2.3.3 Effect of pH

The pH study was next carried out to understand the mechanism of electrochemical oxidation of melatonin. For the study, SWV was recorded in the solution of 25μM melatonin solution prepared using buffer solutions of pH in the range of 2-9. A shift in the peak potential towards lower value was observed with the increasing pH (Figure 4.11,a). This shift of anodic peaks towards a lower potential showcase the facilitation of proton abstraction in basic media[223]. The relation between the peak potential and pH (Figure 4.11,b)can be represented by following linear equation,

$$E_p = - 0.029\ pH + 0.884 \qquad R^2 = 0.99136$$

Being a diffusion controlled process, the oxidation of Mel is assumed to exhibit the nenstian behavior obeying the following equation:

$$E(V) = E^{\circ} - \frac{0.059}{n}\log[\mathrm{H}^{+}]$$

From the Nernst equation expressed above, the slope of E vs pH plot for n = 1 should be 0.059. Therefore, from the slope of the linear equation (dE/dpH) obtained, the number of electrons involved in the electrochemical oxidation of melatonin was found to be ~ 2 (=0.059/0.029) which is in good agreement with the previously reported values.

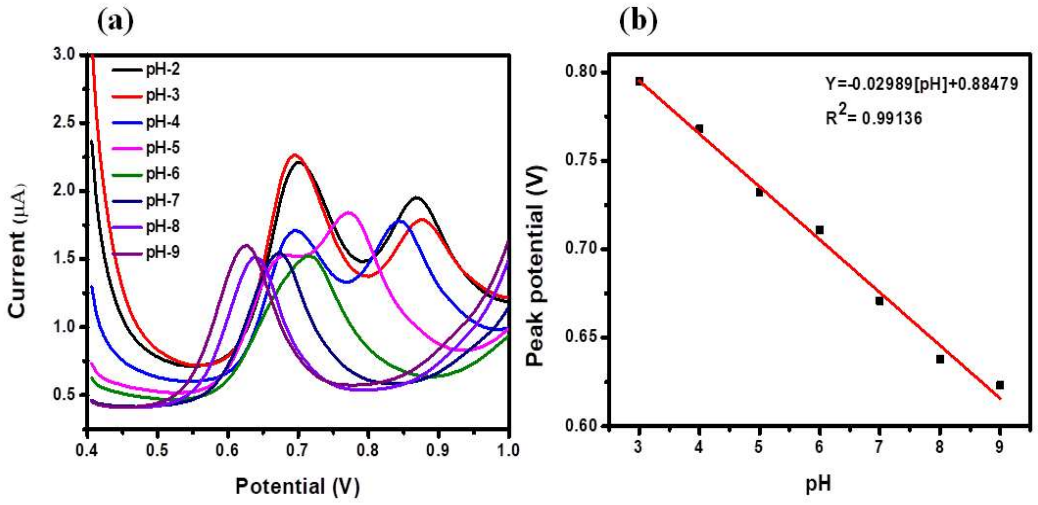

Figure 4.11 (a)Voltammograms for pH of the solution on AuNPs-PLL/PNDs/GCE (b) Effect of pH on AuNPs-PLL/PNDs/GCE

4.2.4 Analytical Application

4.2.4.1 Interference Studies

The estimation of Mel in the complex matrix is majorly challenged by the presence of several other biomolecules like Ascorbic Acid (AA), Uric Acid (UA), and Hypoxanthine (HX) which are commonly present in body fluids as well. Higher concentrations of these metabolites can alter the oxidation peak position and current by interfering in the desired

electrochemical process leading to compromised sensor selectivity. Thus, interference studies have been carried out to investigate the effect of these metabolites.

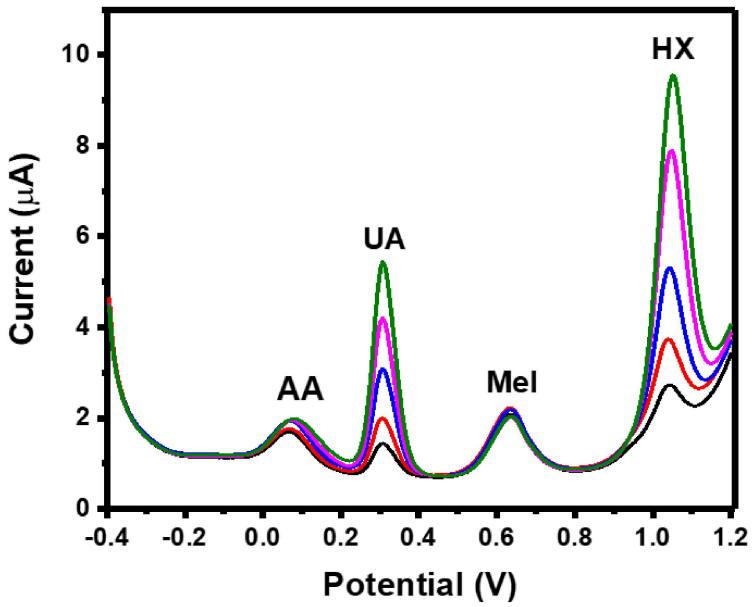

Figure 4.12 Square wave voltammograms were recorded for a fixed concentration of Mel (25μM) with increasing concentration of interference at 12.5μM, 25μM, 50μM, 75μM, 100μM

The SWV voltammograms were recorded for a fixed Mel (25μM) concentration with different concentrations of interference, as shown in Figure 4.12. The AA, UA, and HX oxidation peaks have been observed at 0.06V, 0.30V, and 1.04V, respectively[204]. The recorded voltammograms clearly show that the Mel oxidation peak current and position do not alter even in a high concentration of these interfering metabolites. These results suggest that the modified electrode exhibits promising selectivity and can be used for Mel sensing even in complex matrix and presence of such interfering species.

4.2.4.2 Real Sample Analysis

Pharmaceutical tablet

The modified electrode was utilized to analyze melatonin concentration in the commercially available tablets. For this purpose, a stock solution of 1mM melatonin concentration was made by dissolving the fine powdered tablet in distilled water. The square wave voltammograms were recorded for various tablet concentrations. The table summarizes the observed concentration of melatonin using the calibration chart compared with the sample's actual concentrations. The observed values were found to be in close agreement with the standard concentrations and demonstrated an error of less than 5 %. The concentration, in turn, was also validated using concentration-dependent UV- Vis spectroscopy measurements and exhibited appreciable concurrence with the developed sensor.

Table 4-1 Observed concentration of melatonin using the calibration chart compared with the sample's actual concentrations

Sample	Actual Concentration (µM)	Observed Concentration (µM)	Error (%)
A	25	25.755	3.02
B	50	52.206	4.41
C	100	103.803	3.80

Urine sample preparation

The applicability of the fabricated sensor has been investigated in urine by the standard addition method. Diluted sample (2 ml) of urine was spiked by 500µM stock solution of Mel for desired final concentrations. The square wave voltammograms were recorded with

each spiking of urine shown in Figure 4.13 (a). A weak Mel peak was observed in a diluted urine sample at 0.7V which gets more intense with a gradual increase of Mel concentration. In addition to the Mel peak, the oxidation peak of Uric acid was also observed at 0.4V.

Mung bean Paste

In addition to urine, mung beans paste was also used as a test sample to check the applicability of modified electrode in plants. Crushed mung beans were diluted with pH-7 buffer and directly used for spiking. 2ml of mung bean solution was spiked with a 500µM stock solution of Mel to get the final desired concentration. The square wave voltammograms were recorded with each spiking of Mung bean paste shown in Figure 4.13 (b). Non-spiked mung bean paste showed a small Mel peak at 0.73V with a background peak at 0.86V. The gradual addition of Mel in paste increase the peak current and the calibration plot shows the linear relation between the peak current and Mel concentration. Extrapolation of the obtained cure gives the value of the unknown amount of Mel present in mung bean paste.

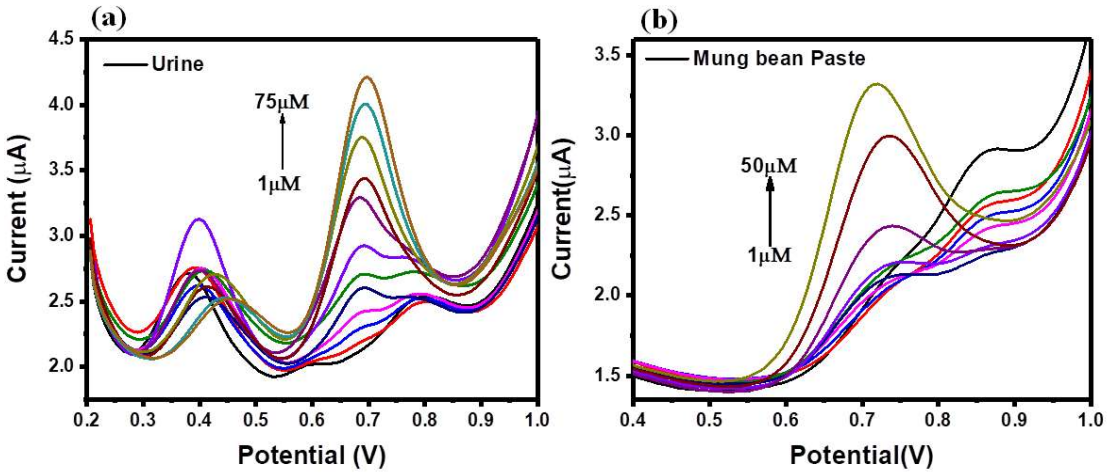

Figure 4.13 (a) Square wave voltammogram of spiked solution of Urine (b) Square wave voltammogram of spiked solution of Mung bean paste

4.2.5 Stability and Reproducibility

The stability of the AuNP-PLL/PNDs/GCE sensing surface was examined by observing the changes in its electrochemical behavior upon excessive cycling in the pH-7 buffer. Figure 4.14 (a) demonstrates the appreciable stability of the fabricated bio-interface over more than 150 cycles. The two peaks observed in Figure 4.14 (a) correspond to the presence of gold nanoparticles and a poly-lysine layer. No substantial change in the shape or the intensity of peaks during the continuous scans confirms the stability of the modified surface for multiple uses. The time-dependent stability and reproducibility of the sensing surface were examined by taking the square wave voltammograms per week in 25µM melatonin solution. The sensing surface showed a < 5 % current drop in the first 15 days and < 9 % after one month when kept open to the air in the lab (Figure 4.14 (b)). The values suggest that the modified surface exhibits excellent stability for a longer duration and does not require extra precautions for storage. However, storing the electrodes in a dry environment or N_2 filled box will increase the lifetime.

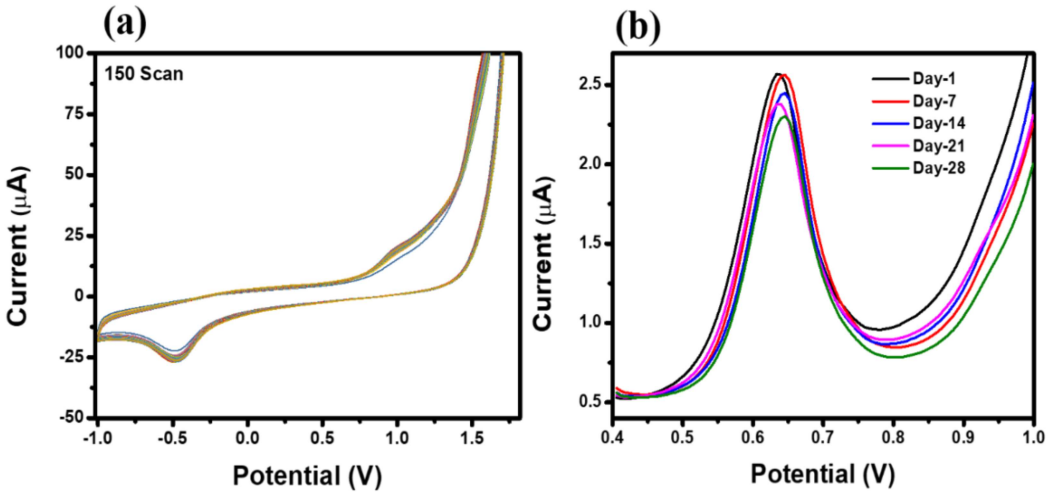

Figure 4.14 (a) Continuous 150 cycle voltammograms of AuNP-PLL/PNDs/GCE (b) Reproducibly of modified sensing surface at different time intervals

4.3 Conclusion

A detailed protocol for the facile fabrication of AuNP-PLL/PNDs/GCE sensor to estimate melatonin has been reported. Utilizing the rich surface functionalities, the BSA derived protein nanodots were electrochemically tailored with AuNP decorated poly-Lysine sheets to overcome their compromised charge-transfer behavior and electrochemical response. The fabricated sensor's chemical and surface characterization has been carried out systematically using HR-SEM, HR-TEM, UV-Vis spectroscopy, FTIR, and XPS. The developed bio-interface was investigated for probing the oxidation mechanism of Mel over electrode surface using CV and SWV. The melatonin was found to oxidize electrochemically, exhibiting a sharp peak at ~ 640mV with a shift of ~ 60mV compared to the oxidation potential of Mel at the bare electrode. The developed sensor demonstrated its efficacy for the quantitative analysis of Mel in a linear range of 0.1 - 200µM with a limit of detection of 31.6nM. The calculated LOD outperformed the previously reported sensors, as summarized in Table 4-2. The as-prepared sensor exhibited excellent selectivity towards melatonin in the test solution, pharmaceutical formulations, and interference matrix. Appreciable stability and reproducibility of the sensor was also evaluated over a period of 28 days. We believe through our work, we open a window for exploring more feasible surface modification strategies to utilize protein-derived nanomaterial for developing stable and selective electrochemical sensors for recognition of biologically relevant molecules.

Table 4-2 Comparison between the performances of reported modified electrodes for melatonin sensing.

Electrode modification	**Standard range**	**LOD**	**Ref.**
Boron doped Diamond electrode	0.5 - 4µM	0.11µM	[208]
ZnO nanorods modified carbon paste electrode	0.3-100µM	750µM	[206]
AHNSA:PdNPs:ErGO/GCE	5 - 100µM	0.09µM	[222]
Palladium nanoparticles decorated carbon aerogel based electrode	0.02 - 500µM	7.1nM	[204]
Cdots/MgNPs/GCE	0.05-13.50µM	0.0044µM	[203]
AB-C modified gold electrode	20-450µM	1.9µM	[205]
AuNPs-PLL /PNDs/GCE	0.1-200µM	31.6nM	This work

Chapter-5

5 Synthesis and Characterization of Novel Protein Nanodots as Drug Delivery Carrier with Enhanced Biological Efficacy of Melatonin in Breast Cancer Cells

5.1 Introduction

Melatonin (N-acetyle-5-methoxytryptamine) (Mel) is an indolic compound with diverse physiological functions[224]. This natural compound, produced primarily from the pineal gland of humans and other mammals, controls the circadian rhythm and sleep-wake cycle, growth, and development of different tissue[225]. Epidemiologic studies revealed that the risk of cancer development inside the body increases with disruption of the natural circadian rhythm and thus with endogenous melatonin rhythms[226]. In females, disrupted natural circadian rhythm induced breast cancer development is very common[227]. Endogenous Mel modulates several signal transduction pathways associated with cell survival, migration, proliferation, and apoptosis[228] by counter-checking the redox status of the cells and thus act as checkpoints of the actions of several oncostatic factors[229,230].

Moreover, Mel is a potent antioxidant with anti-inflammatory and antitumor properties and is used as a therapeutic agent for treating diverse types of cancers[231–234]. A cancer patient on Mel medication frequently takes Mel into the body due to its high oxidation affinity, short half-life (~ 35-50 min), and slow dissolution properties. Mel gets metabolized easily and get eliminated fast from the patient's body[235–239]. Mel conjugated with nanocarriers gets released slowly over a more extended period, thereby reducing the dosage and

improving its bioavailability to cancer cells[240–244]. Different kinds of nanocarriers like chitosan-tripolyphosphate nanoparticles, polyethylene glycol microspheres (PEG), PLGA nanoparticles, gold nanoparticles (AuNPs), etc., have been used for oral, intravenous, and transdermal application of Mel[242,245–247]. The limitations of previously reported nanocarriers are their multistep synthesis process, large size, higher cost of production, difficulty in scaling up, unexpected changes in pharmacokinetic behavior, toxic side products, accumulation in the body, heterogeneous phenomenon, poor drug loading, and high burst release rate of the drug and so on [123,248–252].

In recent years, fluorescent nanomaterials have been in high demand for basic and industrial research due to their potential applications in bioimaging, sensing, and drug delivery[253–256]. Several materials and methods have been used to synthesize fluorescent nanomaterials[81,257,258]. For the last two decades, carbon quantum dots (CQDs) has been explored as a fluorescent material for different applications[259,260]. However, in the synthesis process of carbon quantum dots, toxic heavy metals (e.g., cadmium, lead) are involved, limiting their widespread use in *in vivo* biological applications[261,262]. The major concerns with the present fluorescent materials are their size, low quantum yield, generation of chemical waste, multi-step process, and bio compatibility[263]. These concerns have restricted the wide-scale biological application of available fluorescent materials, especially *in vivo*, which has fueled the search for alternative nontoxic and environment-friendly nanoparticles for bioimaging and drug delivery[124].

As an alternative, fluorescent nanodots synthesized from bio-molecules like DNA, nucleotides, and carbohydrates have received increased interest due to their characteristics like excellent biocompatibility, facile synthesis method, water-solubility, high photostability, low cost, higher life-time[264–266]. In particular, nanodots are effectively

employed in biomedical applications based on their robust and tunable photoluminescence properties. Due to their beneficial aspect and enormous applications, it is necessary to devise efficient and straightforward routes for synthesizing other fluorescent nanodots of biological origin to improve their applications in *in vivo* conditions.

In the present study, biocompatible green-emitting protein nanodots (PNDs) having robust and tunable photoluminescence properties were synthesized from a common model protein lysozyme by a one-step hydrothermal method. The synthesis of PNDs as a drug carrier was optimized and used as a novel nano delivery system for melatonin in the breast cancer cell. They also enhanced the efficacy of the drug melatonin by slow but sustained release in breast cancer cells. Further, it has been exploited as a bioimaging tool even at higher melatonin concentrations, as no fluorescence quenching was observed. This makes it an ideal candidate for drug delivery and bioimaging tool in the biomedical field for *in vivo* study.

5.2 Results and Discussion

5.2.1 Synthesis and Characterization of the Synthesized PNDs

Protein nanodots were synthesized using a common model protein lysozyme to synthesize a novel drug delivery carrier with enhanced biological efficacy. We demonstrate that these PNDs have excellent fluorescent properties, are biocompatible, and have various functional groups, making them ideal for bioimaging and drug delivery. The overall synthesis process and mechanism of formation of PNDs were schematically presented in Figure 5.1. Above the melting temperature, the native structure of protein deform, leading to the construction of the small peptide strands. Further increase in temperature starts to break peptide strands in carbonaceous core nanostructure form with functional activity via self-assembly[267]. A

previous report suggested that temperature and time duration in hydrothermal technique play a significant role in forming the nanodots by controlling the particle size, which further enhances photoluminescence [268,269]. For a short period, heating at lower temperatures may not lead to appreciable carbonization of organic material to produce fluorescence [270]. So, we used a high temperature (200°C) with a longer duration (15 h) to synthesize PNDs. Above 70°C, lysozyme completely melts in all pH ranges, but the conformation of folded protein depends on pH [271]. To understand the effect of conformation of folded protein on the properties of the synthesized PNDs, PNDs were synthesized at two different pHs (pH-2 and pH -7). During the hydrothermal process, native proteins at both pHs were heated at 200^0C for 15 h to disrupt the non-covalent bonds responsible for stabilizing the lysozyme. These PNDs were then extensively characterized using spectroscopic, optical, and microscopic techniques.

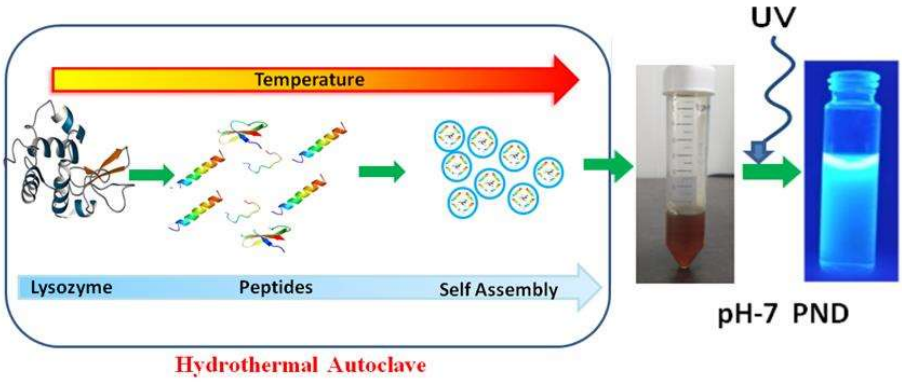

Figure 5.1 Schematic presentation of synthesis of PNDs using hydrothermal method

The UV-Vis absorbance spectrum reveals maximum absorption in the UV-blue region with two prominent absorbance peaks at 275 nm and 330 nm (Figure 5.2a). Absorbance at 275nm is ascribed to π -π * electronic transition of C=C and n-π * electronic transition of

C=O presence on PNDs surface.[272273] The broad absorption extended from 330-350nm is due to the excited states of functional groups on the surface.[274275] One of the most remarkable characteristics of PNDs is their intrinsic photoluminescence property. It has an excitation-dependent fluorescence spectrum with maximum fluorescence intensity when excited at 340nm (Figure 5.2b). Wavelength-dependent emission in nanodots can be attributed to the non-uniform size distribution of PNDs and the presence of various surface functional groups like carboxyl, hydroxyl, and other oxygen species. The fluorescence lifetime of PNDs at room temperature was measured with an average lifetime of 2.77 ns by fitting with an R^2 value of 0.995 (Figure 5.2c), where τ_1=2.23 ns, τ_2= 5.94 ns. Multiexponential emission decay may arise from rapid bandgap transitions between different discrete states or may also indicate the fast radiative recombination of multiple exciton species contributed by carboxyl, hydroxyl, and other oxygen species.[264] It has been reported that higher nitrogen doping in nanodots usually leads to a longer lifetime.[276] Larger lifetimes at excited energy levels make PNDs an excellent material for cell imaging and fluorescent-dependent sensing. Using Equation 5.1 relative quantum yield of PNDs was calculated (Figure 5.2 (d)) and was found to be ~14 % for pH-2 and ~22% for pH-7 PNDs and using quinine sulfate as a reference in 0.1M H_2SO_4.[277]

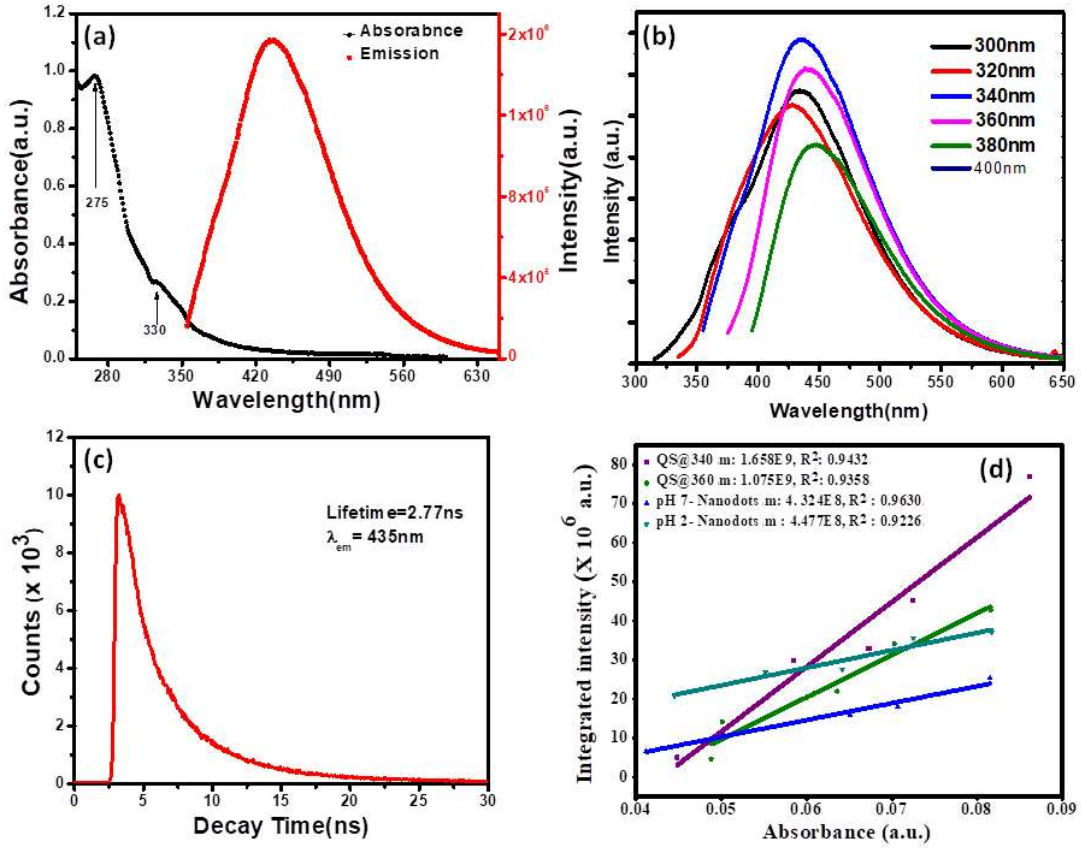

Figure 5.2 Optical Characterization of pH-7 PNDs (a) UV-Vis absorption and emission spectra (λex = 340nm) of an aqueous dispersion of PNDs (b) Excitation wavelength-dependent emission of PNDs (c) Time-resolved PL decay curves of PND (λem =435 nm) (d) Quantum yield calibration plot

XPS and FTIR studies were conducted to gain information about the chemical composition and functional groups on the surface of PNDs. The bands at 3418 cm^{-1} and 3186 cm^{-1} are due to stretching vibrations of the O-H bond of the phenolic group and the N-H bond of the amine(-NH_2) group, respectively (Figure 5.3 a). The presence of many O-H and N-H groups lends to the hydrophilicity of PNDs. The broad peak between 1500-1700 cm^{-1} is composed of stretch vibration of C=C bonds, C=N bonds, and N-H bond of amine groups. The presence of graphitic nitrogen bonded to three carbon atoms (C=N) is indicative of nitrogen doping of the carbon core of PNDs. The peaks around 1404 cm^{-1} and 1109 cm^{-1} are stretch vibrations of C=O bond carboxylic groups and C-O bonds.[278] The characteristic

amide I (stretching of C=O) and amide II band (bending of the N–H and stretching of the C–N group) of protein is not observed at all, indicating all the lysozyme has decomposed to form nanodots. XPS survey scan of PNDs shows that the PNDs are mainly composed of carbon, oxygen, and nitrogen (Figure 5.3 b). The high-resolution C1s (Figure 5.3 c) spectra have been deconvoluted into three components corresponding to the C=O group (288 eV), C–N group (286 eV), and C–C (284.8eV). The N1s spectrum (Figure 5.3 d) has been fitted with two peaks at 399.6 and 400.3 eV, which are assigned to N–C and N=C groups, respectively. The high-resolution O1s (Figure 5.3 e) spectrum contains a peak at 531eV & 531.6, r due to the presence of O-H & C=O groups, respectively. The higher percentage of nitrogen than oxygen on the PND surface leads to the high fluorescent intensity at a very low concentration in an aqueous solution. Both XPS and FTIR measurements complement each other and confirm the presence of oxygen-containing functional groups and nitrogen-containing amino groups on the PNDs surface.

Transmission electron microscopy (TEM) was employed to estimate the size and morphology of the PNDs. PND diameter lay within 3-5 nm with an average diameter of around 3.5nm (Figure 5.4 a). Zeta potential measurement of the synthesized PNDs at pH-2 and pH-7 showed negative surface zeta potential of 17.4 mV and -12.5 mV, respectively (Figure 5.4 b). The higher negative values of zeta potential show the stability of PNDs in an aqueous solution owing to electrostatic repulsion between individual PNDs.[279]

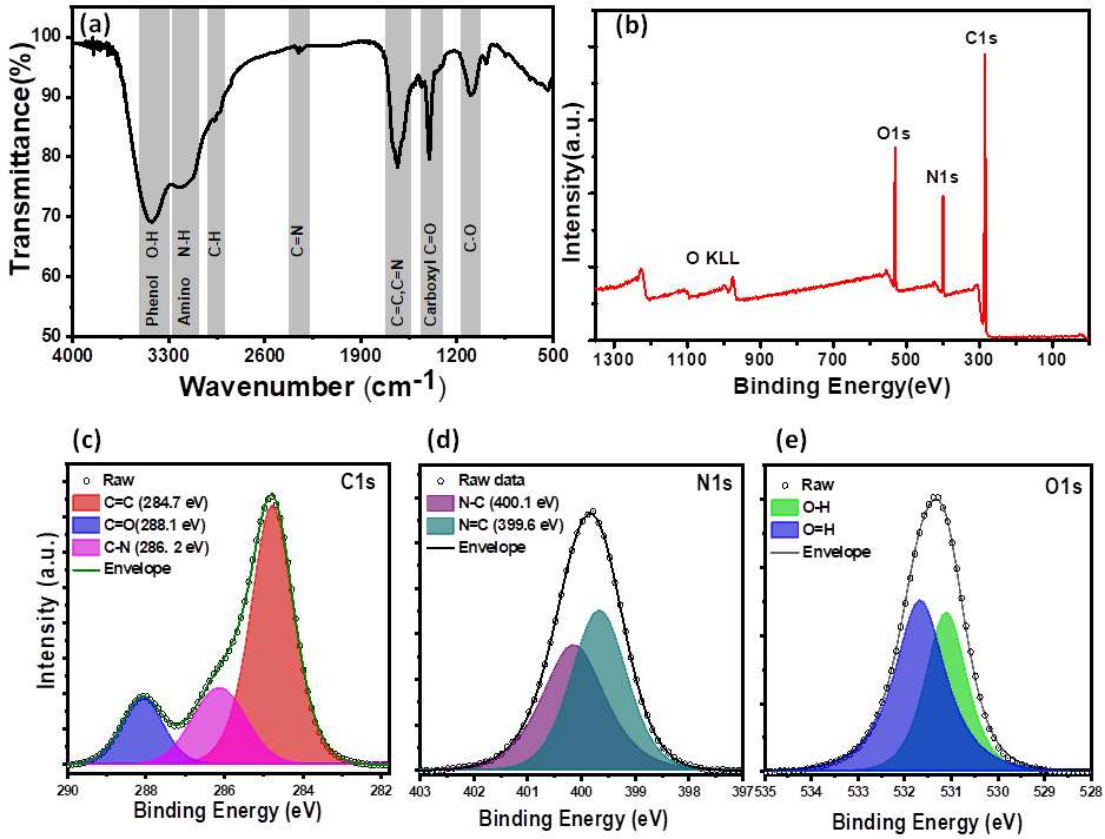

Figure 5.3 Spectroscopic characterization of PNDs (a) FTIR spectrum of PND (b) XPS Survey spectrum (c)-(e) High-resolution XPS spectra of C1s, N1s, and O1s. The XPS peaks have been deconvoluted into several components

5.2.2 *In vitro* Cell Cytotoxicity Study of PNDs

Physical characterization of the PNDs suggested that it is an excellent fluorescent carrier for bioimaging. On the other hand, a wide range of functional groups on its surface makes it an efficient nanocarrier with higher drug loading efficiency. To be an efficient drug carrier for biological applications, the PNDs should be biocompatible with no/minimal cellular toxicity. We first studied whether the PNDs of both pHs (pH-2 and pH-7) are non-toxic to the cells using an MTT assay. At pH=2, the MTT assay for different concentrations of PNDs showed cell death (3% - 21%) in MG63 at all studied concentrations (Figure 5.4 d). One possible reason could be that cell has a low survival rate at acidic pH. Contrary,

when we analyzed the cytotoxicity of pH-2 PNDs in a pH-7 buffer solution, cells showed 99% survival (Figure 5.4 d). This shows the importance of pH in cell cytotoxicity studies and confirms the fact that cells are more viable at pH-7. Similarly, we analyzed the toxicity of pH-7 PNDs using different concentrations (Figure 5.4 c). The result showed only 3-0.6% cell death, which was very low compared to pH-2 PNDs. Thus, we can say that PNDs synthesized at pH-7 are less cytotoxic.

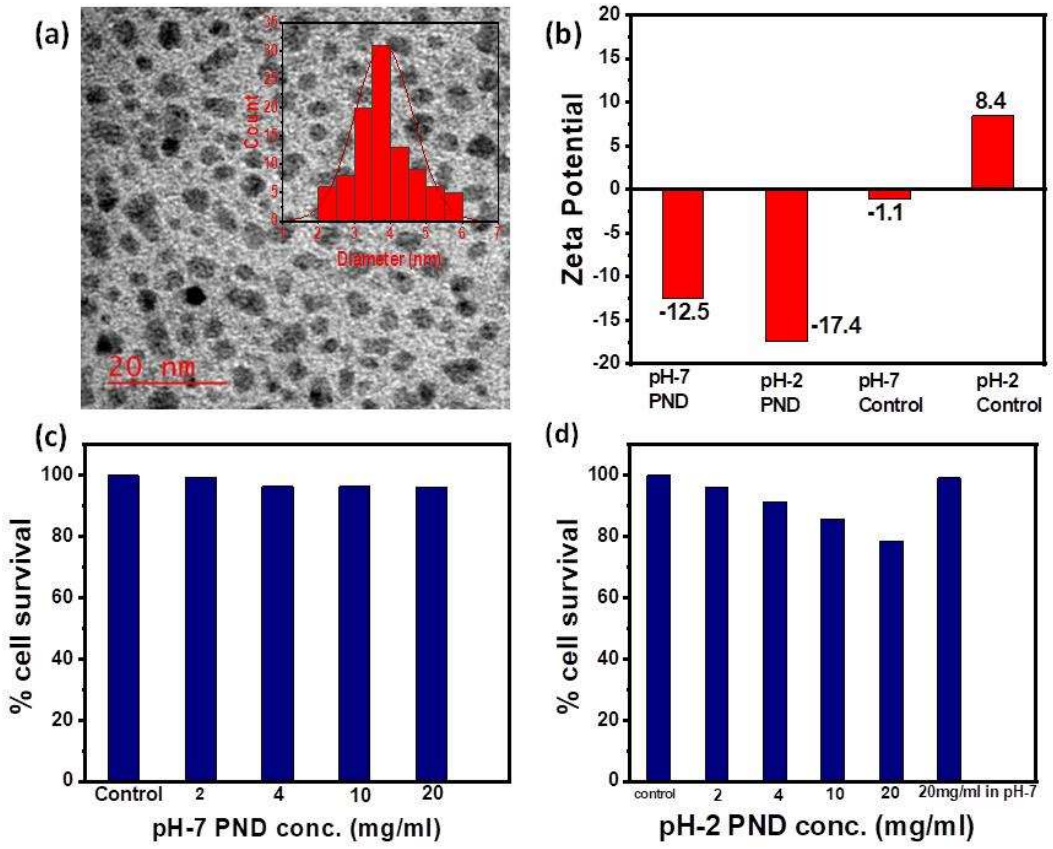

Figure 5.4 (a) TEM of PNDs, Histogram of particle size distribution is shown in inset (b) Zeta Potential of PNDs (c) Concentration-dependent cell viability of PND for 24h (d)) Concentration-dependent cell viability of pH-2 PND for 24hr

PNDs synthesized at pH-2 were showed similar physicochemical properties as pH- 7 PNDs, which suggests that both the PNDs have similar morphology and chemical composition.

The optical characterization studies of pH-2 PNDs are shown in Figure 5.5. pH-2 PNDs show the characteristic absorbance peak at 268nm with a maximum emission wavelength of 448nm. TEM images confirm the spherical morphology with homogenous particle distribution. The histogram present in the inset of Figure 5.5 (b) shows that most of the PNDs have particle size distribution between 3.5nm, which is similar to pH-7 PNDs. The excitation wavelength for maximum emission for pH-7 PNDs was 340nm, whereas, for pH-2 PNDs, it was 360nm. The differences in the ratio of functional groups present on the surface and defects can be the reason for this redshift in wavelength.

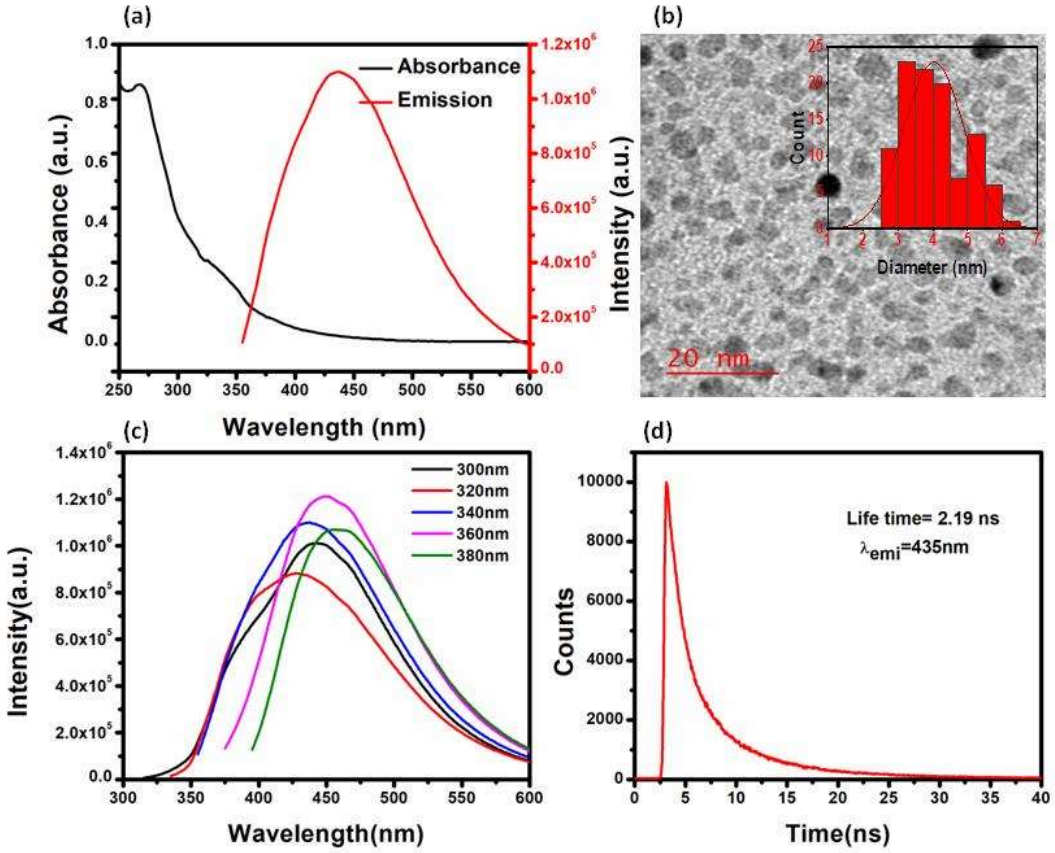

Figure 5.5 Optical characterization of pH-2 PND (a) UV-Vis spectra and Emission spectrum at 340nm (b) TEM images of pH-2 PND; Histogram shows the particle distribution (c) Wavelength dependent emission spectra (d) Time-resolved PL decay curves of pH-2 PND (λem =435 nm)

The peaks present in the fingerprint region of the FTIR spectrum (600-1400cm^{-1}) are related to the composition of the surface. The comparative studies of the FTIR spectrum of pH-2 PNDs and pH-7 PNDs show nanodots have similar surface functionality. The FTIR spectrum of pH-2 PNDs (Figure 5.6 a) shows the characteristic peaks of the same functional groups present in the pH-7 PNDs spectrum. The detailed analysis of the XPS spectrum (Figure 5.6 b-d) also confirms the same elemental composition in both PNDs with an insignificant shift in binding energy.

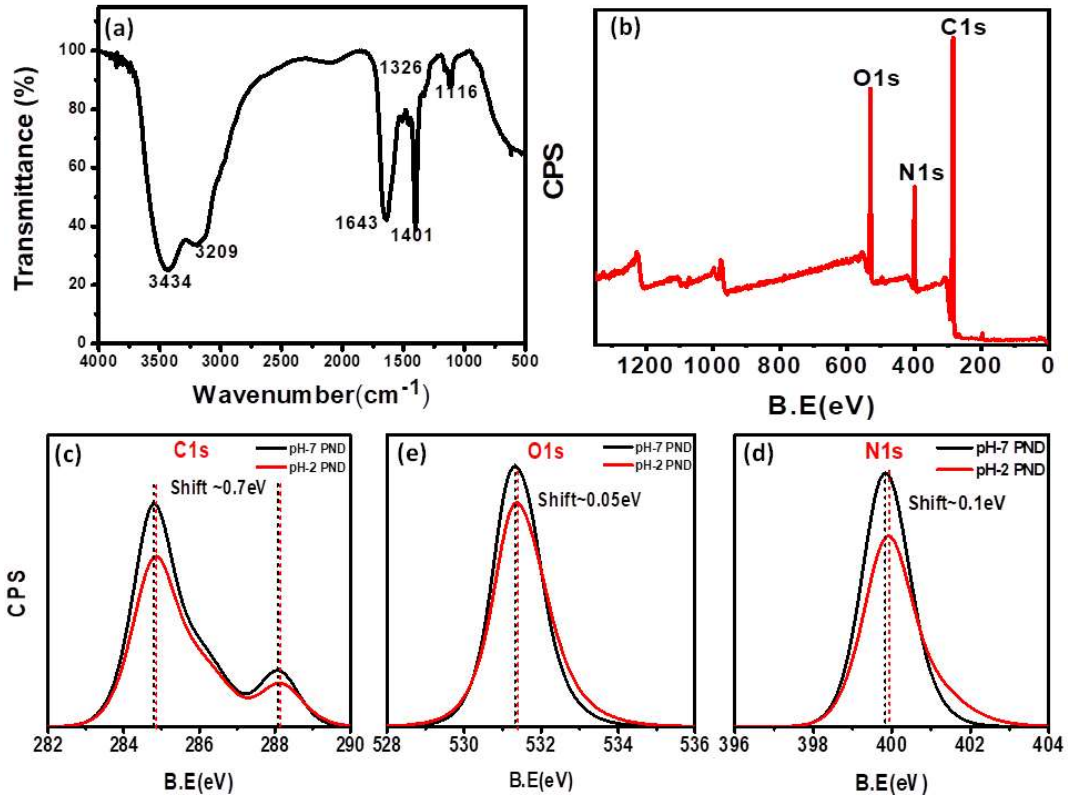

Figure 5.6 (a) FTIR spectrum of pH-2 PND (b) Full scan XPS spectrum of pH-2 PND (c)-(d) shows the comparative shift in the peak position of C1s, O1s, and N1s of pH-7 and pH-2 PND.

5.2.3 PNDs as a Fluorescent Tool for Bioimaging Studies

In recent years, the nucleus has been considered a diagnostic biomarker for pre-monitoring diseases like cancer and cellular stress conditions due to changes in its morphology like nuclear fragmentation, nuclear blebbing, and nuclear size.[239] In addition to the MTT assay, the biocompatibility of PNDs (pH-7 and pH-2) was studied by fluorescence microscopy. The concentration-dependent fluorescence studies of pH-2 and pH-7 PNDs are shown in Figure 5.7 and Figure 5.8.

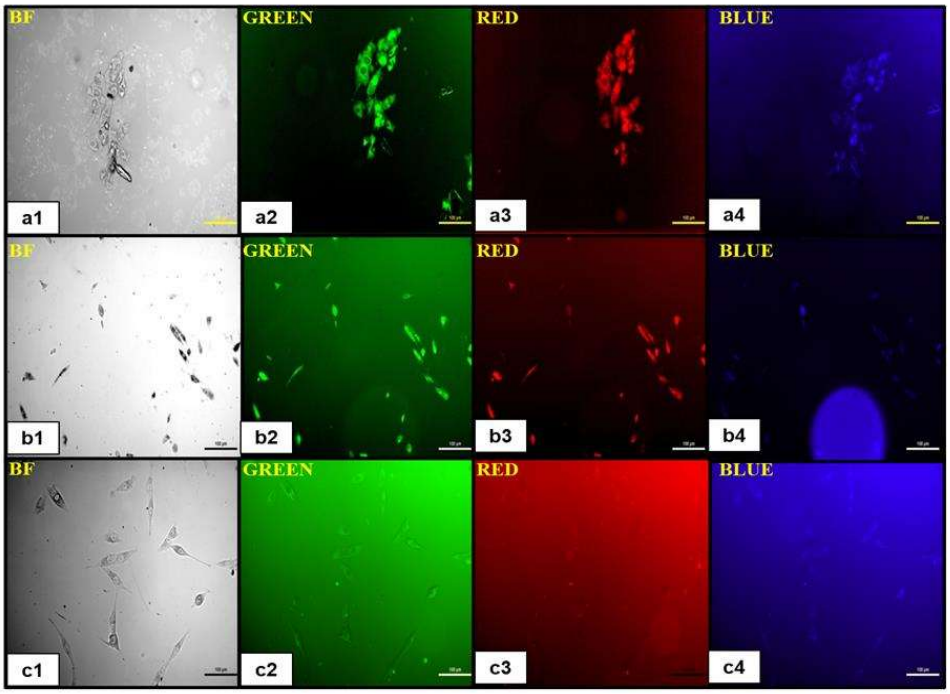

Figure 5.7 Fluorescence imaging of pH-2 PNDs in different concentrations (a1-a4: 20mg/ml; b1-b4: 10mg/ml; c1-c4: 4mg/ml) in MDA-MB-231 breast cancer cells

The intensity level of fluorescence of both PNDs was studied at different concentrations. Results showed high fluorescence at 20mg/ml concentration in both pH-2 and pH-7 PNDs, whereas at 4mg/ml (low) concentration pH-2 PNDs showed no fluorescence from the cells,

while pH-7 PNDs still showed minimum fluorescence (Figure 5.7 (a1-a4), (b1-b4), (c1-c4) and Figure 5.8 (a1-a4), (b1-b4), (c1-c4)). Therefore, for further studies, pH-7 PNDs were used at 20mg/ml concentration as a fluorescent nanocarrier for the bioimaging and drug delivery of the Mel.

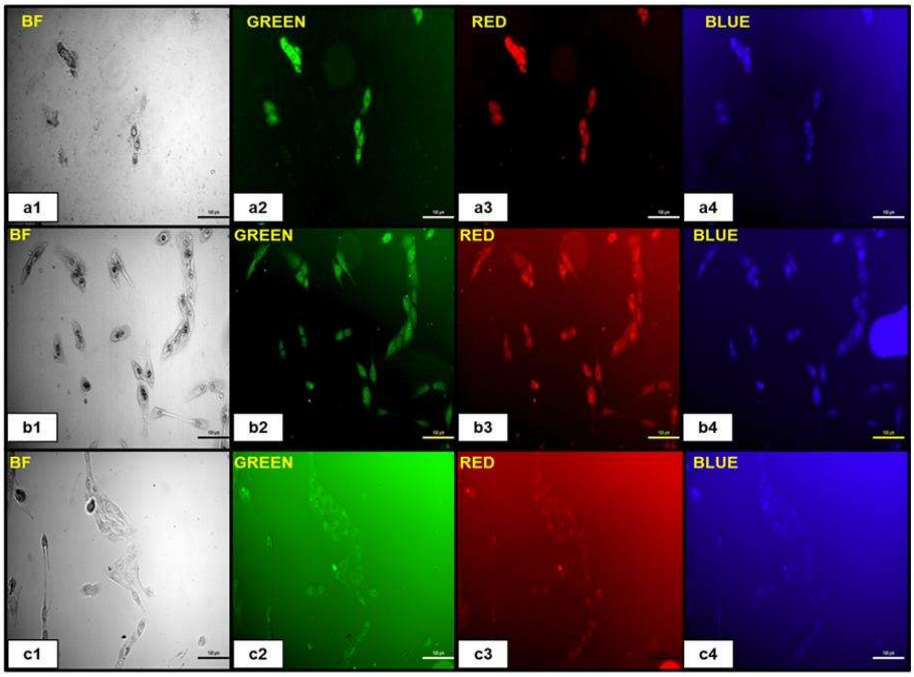

Figure 5.8 Fluorescence imaging of pH-7 PNDs in different concentrations (a1-a4: 20mg/ml; b1-b4: 10mg/ml; c1-c4: 4mg/ml) in MDA-MB-231 breast cancer cells

5.2.4 Physical characterization of Mel loaded PNDs (MPNDs)

The optical characterization of Mel shows an absorbance peak at 275nm. The excitation and emission spectra showed that both excitation wavelengths (260nm and 313nm) correspond to the same emission range with a peak position at 356nm (Figure 5.9 a). pH-7 PND and Mel conjugate (MPNDs) are stable in water suspension for several months without changing their optical properties. By analyzing the absorbance peak of Mel and emission peak of PNDs, we can conclude that no Fluorescence Resonance Energy Transfer

(FRET) phenomenon is happening between PND and Mel.[280] The FTIR spectrum of a pure MEL standard showed major peaks of functional groups at 3306 and 3260 cm^{-1} (N–H bending and C–N stretching), 1492 and 1550 cm^{-1} (aromatic –C=), 1630 cm^{-1} (C=O), 1180 and 1217 cm^{-1} (–C–O) and the complex formed with PNDs shows a slight shift in peak positions (Figure 5.9 b).[123] FTIR study shows that functional groups present on the PNDs surface, mainly double bonds(C=O, C=C, and phenolic groups), can interact with the aromatic ring of Mel with dipole-induced dipole forces and form a complex which can facilitate charge transfer from donor to acceptor. The complex shows a higher increase in fluorescence intensity at a very low concentration of Mel. As we increase the concentration of Mel in the system, intense fluorescence remains constant (Figure 5.9 c). Mel interaction with PNDs provides new states and defects for charge transfer and enhances photoluminescence intensity.[280,281] UV and PL analysis of the complex shows that PNDs can be an excellent carrier for bioimaging and drug delivery of Mel for further *in vitro* studies.

5.2.5 Studying the therapeutic bio-efficacy of Mel loaded PNDs (MPNDs)

In order to study and understand the biological efficiency of MPNDs for breast cancer treatment, first, we measured the IC_{50} of the alone Mel drug in MDA-MB231 cells, which was 0.84 mM, and this concentration was further used for all drug treatments in the present study. Mel was then loaded in PNDs, and MPNDs were prepared at 0.84 mM concentration (Figure 5.9 d). The IC_{50} values of Mel have been shown in parabolic and linear graphs in Figure 5.10 (a,b).

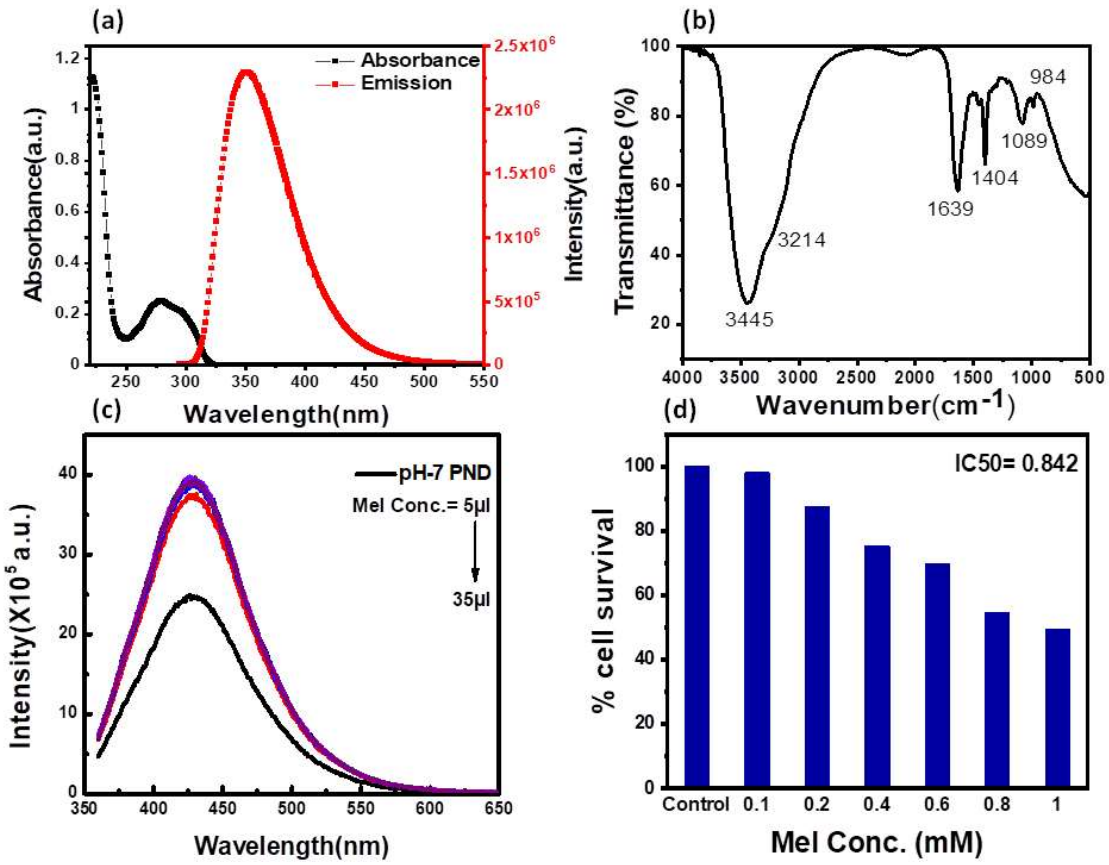

Figure 5.9 (a) UV-Vis and emission spectra of melatonin, (b) FTIR spectrum of pH-7 PNDs and Mel-pH-7 PNDs (MPNDs) and (c) Emission spectra of Mel-pH-7 PNDs (MPNDs) at increasing concentration of Mel, (d) Cell viability study of dose-dependent Mel for 24h

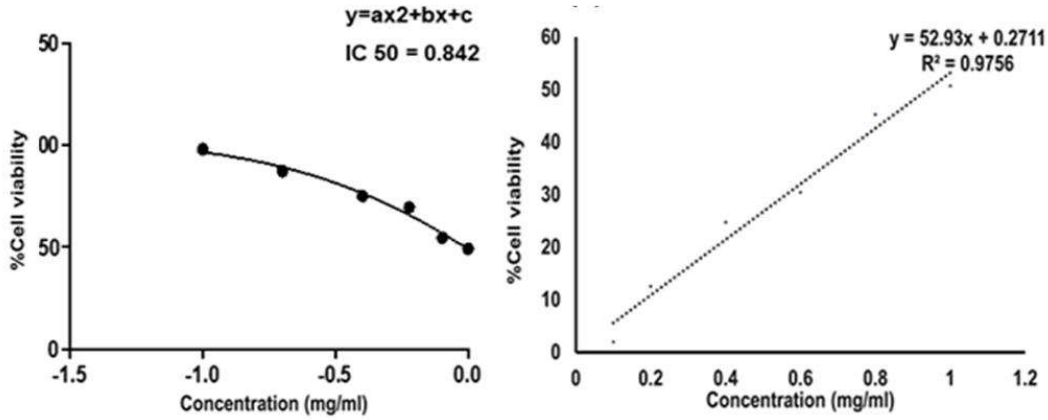

Figure 5.10 (a) Parabolic graph and (b) linear graph of Mel dose-dependent cell survival for IC50 value analysis.

pH-7 PNDs confirmed its permeability through confocal imaging in both cytoplasm and nucleus (Figure 5.11, b1-b4) and thus enhanced the possibility of nuclear drug delivery applications. The maximum fluorescent intensity and minimum cell death were recorded for 20mg/ml concentration of pH-7 PNDs, which were used for further biological studies. MDA-MB231 cells were treated with Mel and MPNDs separately and incubated for 24h. Physical characterization of Mel showed negligible self-fluorescence at the cellular level. Thus, cells treated by Mel only showed no fluorescence (Figure 5.11, c1-c4). On the other hand, PNDs and MPNDs allowed visualization of morphological changes after treatment in confocal imaging (Figure 5.11, d1-d4).

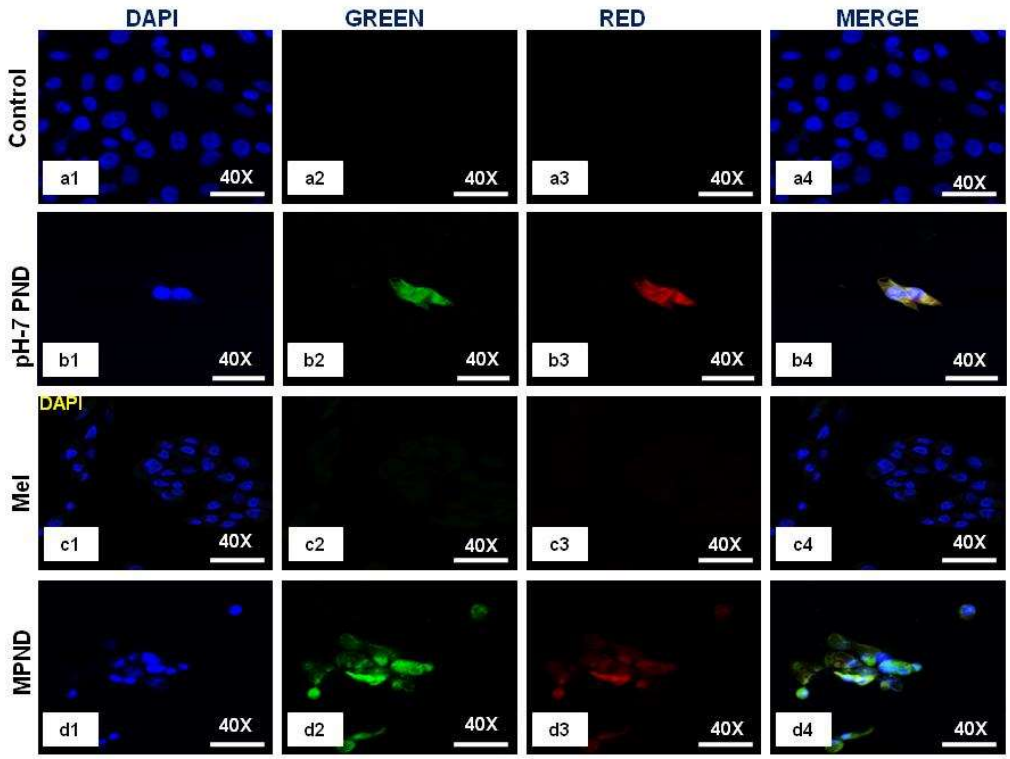

Figure 5.11 Confocal images of breast cancer cell control (a1-a4) and treated with pH-7 PNDs (20mg/ml:b1-b4), only Mel (0.84mM:c1-c4) and Mel-pH-7 PNDs (MPNDs) (0.04mM +20mg/ml pH-7 PNDs:d1-d4).

Cell proliferation analysis via MTT assays after 24h, 48h and 72 h incubations with Mel only and MPNDs separately showed a significant decrease in cellular mortality in both groups up to 48h of treatment compared to control and only PND treated cells. Interestingly after 72h of treatment, Mel treated cells showed less cell mortality (31.33%), whereas MPNDs still showed high cell mortality (61.53%). From these results, we may conclude that MPNDs might have helped in the slow release of the drug, making it more effective for a longer time, i.e., 72h (Figure 5.12).

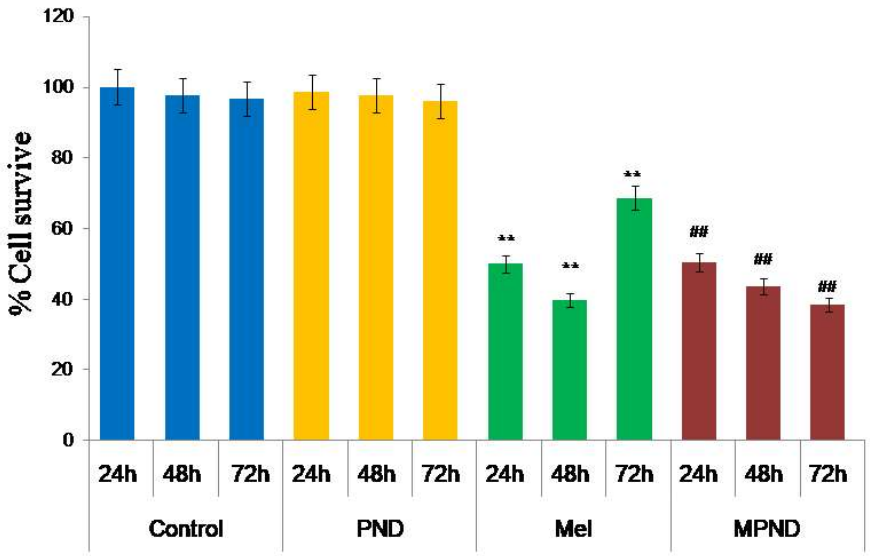

Figure 5.12 Cell proliferation analysis with Mel and MPNDs by MTT assay, ** showed the significance level of $p<0.001$ between control and Mel, whereas ## showed the significance level of $p<0.001$ between Mel and MPND

Various nano-carriers have already been reported for drug delivery of Mel effectively in cancer therapies. Maximum on them possesses self-toxicity towards the cancer cells, which enhances the mortality efficacy of Mel in *in vitro* cancer treatment with time.[123,282] But this self-toxicity of nanocarriers can also harm other than cancerous cells of the body.

Importantly our synthesized PND was non-toxic and thus, the retained cell mortality of MDA-MB231 cells for at least 72h was totally due to the slow release of the drug Mel from MPND.

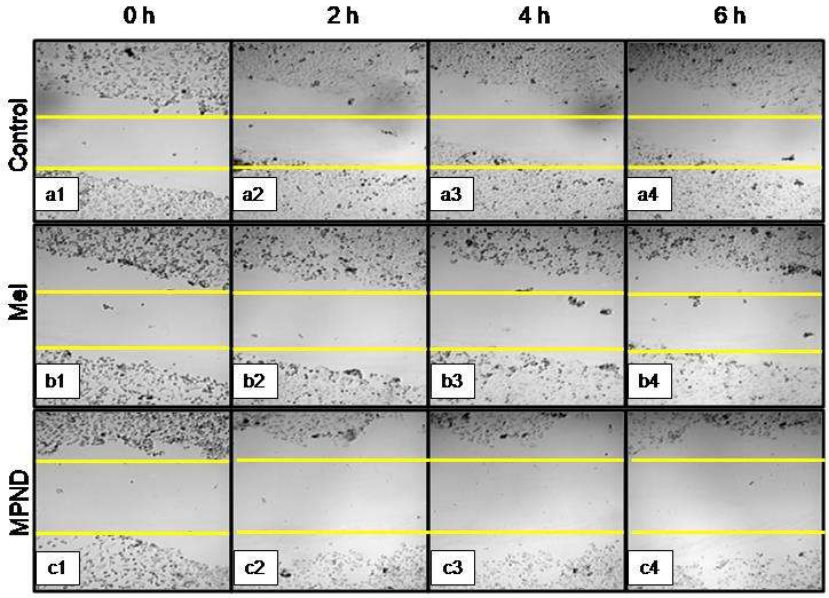

Figure 5.13 Cell migration study with Mel (b1-b4) and MPNDs (c1-c4)

Cell migration is involved in several pathological processes such as tumor invasion, neoangiogenesis and metastasis. To study the efficacy of MPND as compared to Mel alone on cell migration, we performed the *in vitro* wound-healing assay. We found that breast cancer cell migration becomes slower with Mel treatment and also cell death was also observed from the wound site at the time interval of 4h and 6h compared to control cells. In comparison with only Mel treatment, MPNDs treated cells showed no cell migration at the time interval of 2h and 4h and very small cellular progression towards the wound at 6h was observed. Simultaneously, higher cell death was observed in the MPNDs treated cells at the wound sites at 2h, 4h and 6h (Figure 5.13). The histogram shows the statistical

analysis of the cell migration assay in Figure 5.14. These results support previous views of melatonin in breast cancer treatment with the added benefit that MPNDs lower the limitation of the half-life of Mel which enhance the efficiency of Mel in reducing cell proliferation and cell migration.[283,284]

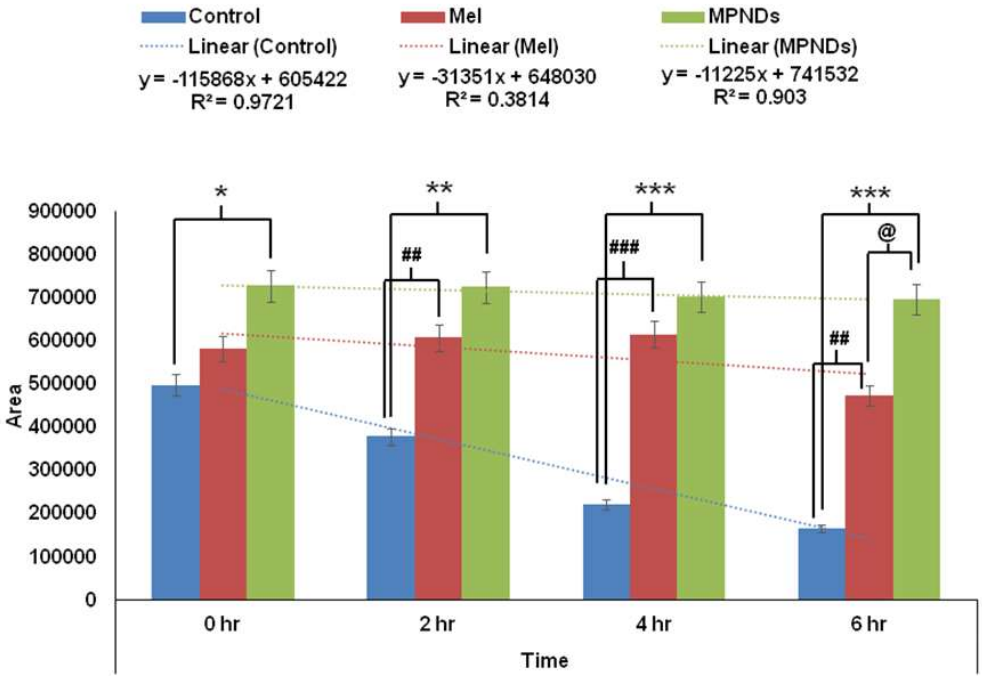

Figure 5.14 Histogram showing the wound closure % within-group comparison; * denotes significant changes between control and MPNDs groups; # denotes significant differences between control and Mel groups and @ denotes significant changes between Mel and MPNDs groups

5.3 Conclusion

In the present study, we have reported an efficient, simple and cost-effective method for synthesizing protein nanodots (PNDs) at two different pHs using lysozyme as a protein source. Synthesized PNDs were thoroughly characterized using TEM, FTIR, UV-Vis, and XPS for morphological and chemical analysis. Further, synthesized PNDs were used as a carrier for loading of melatonin and synthesized MPNDs nano-drug delivery system was

characterized. They showed remarkable aqueous stability and photoluminescence property. The application of developed MPNDs was studied on breast cancer cells. MPNDS showed higher cellular uptake, more cytotoxicity and invasion properties than free melatonin. Thus, a novel nano-drug delivery system for melatonin breast cancer cells was successfully synthesized and applied as efficient bioimaging and drug delivery system.